[6] Cassanova, R. A., "Expansion of a Jet into a Vacuum," *Eleventh International Symposium on Combustion*, Univ. of California, Berkeley, Calif., 1966.
[7] Love, I. S. et al., "Experimental and Theoretical Studies of Axisymmetric Free Jets," TR-R-6, 1959, NASA.
[8] Shapiro, A. H., *The Dynamics and Thermodynamics of Compressible Flow*, Vols. I and II, Roland Press, New York, 1953.
[9] Pack, D. C., "On the Formation of Shock Waves in Supersonic Gas Jets," 1947, Univ. College, Dundee, Scotland.
[10] Stechman, R. C. et al., "Hydrazine Monopropellant Rocket Engine Plume Tests," Internal Report 79, June 1967, Rocket Systems Div., The Marquardt Corp., Van Nuys, Calif.

FEBRUARY 1970 J. SPACECRAFT VOL. 7, NO. 2

Swirling Flow through a Nozzle

JAMES L. BATSON*
U.S. Army Missile Command, Redstone Arsenal, Ala.
AND
RICHARD H. SFORZINI†
Auburn University, Auburn, Ala.

This paper presents the results of an experimental investigation of swirling flow through a nozzle. Its purpose is to determine the effect of swirl on the flowfield, thrust and mass flow produced by nozzled devices. Swirling flow is induced by injecting cold gas tangentially to a cylindrical chamber wall. The internal flow characteristics are determined by use of miniature probes. Liquid injection provides a means of flow visualization. Nozzle exhaust flow is examined by a shadowgraph. Thrust and mass flow rates are obtained for four swirl conditions and related to axial flow theory and to Mager's solution of isentropic swirling flow. The results have implications with respect to performance of spinning rocket motors.

Nomenclature

a_o = total speed of sound
M, M_I = mass flow and axial isentropic mass flow
P_C, P_{OC} = static and stagnation pressures in the chamber
P_O = stagnation pressure of inlet flow
R = radius of cylindrical chamber
r = radius of position in flowfield
r_C = radius of exhaust core measured at exit plane
r_e = radius of nozzle exit
r^* = radius of nozzle throat
T_C, T_{OC} = static and stagnation temperatures in the chamber
T_O = stagnation temperature of inlet flow
V = tangential velocity in the chamber near the wall at station 2
v = tangential velocity
α^* = Mager's swirl parameter $= RV[(\gamma - 1)/2]^{1/2}/r^* a_o$
γ = ratio of specific heats (for air = 1.4)
ρ_c = static density in the chamber
ρ_o = stagnation density of inlet flow

Introduction

SWIRLING flow occurs in many rockets (especially spin-stabilized rockets), jet engines, plasma jets (to stabilize the arc), vortex valves, industrial furnaces (vortex burners), and cyclone separators. Despite the interest created by these applications, the mechanics of swirling flow are not clearly understood, especially with respect to the passage of the flow through a nozzle.

Spin produces swirling flow within a solid-propellant rocket motor (SRM) by imparting angular momentum to the gas evolving from the surface of the burning grain. Because of the conservation of angular momentum, the swirling motion becomes very intense in the nozzle throat, as does the motion of a spinning ice skater who brings his arms down to increase his spin. The axial movement of the gas is impaired, so that the effective throat area is reduced. The chamber pressure will tend to increase because of the inability of the nozzle to pass the mass generated in the SRM at a lower pressure, resulting in a higher burning rate and, to satisfy continuity relations, in a new and higher equilibrium operating pressure. The action of swirling flow on the burning surface of the propellant can cause grain erosion aggravating the situation. These events coupled with the effect of centrifugal force on the combustion mechanism of the propellant may cause the chamber pressure to exceed the structural limits of the motor case, ending in catastrophic failure. In a liquid-propellant rocket the effective throat constriction can also result in significant changes in operating conditions, unless a control system compensates for it.

To date, little information has been published on measured effects of swirl upon mass flow and thrust. It is impractical to probe the flow within an SRM rotating at 3000 to 20,000 rpm, and it is difficult to isolate the effect of swirling flow through the nozzle. The method of inducing swirl used in this research was injection of cold gas tangentially to a cylindrical chamber wall as in the vortex or Ranque-Hilsch tube.[1-5] This method of producing swirl was advantageous in that no moving parts were required, thus facilitating the measurement of the internal flowfield. Although the properties of cold gas do not match the properties of the hot gas in a rocket, and the character of the energy equation differs between cold and hot gas, the results provide a means for basic understanding of swirling flow.

The nature of the vortex formed within the Ranque-Hilsch tube is that of a free or potential vortex. One would also expect this type of flow to be a characteristic of the flow within an internal-burning SRM. The spinning of the propellant surface in an SRM imparts a tangential velocity to the flow, whereas in the experimental apparatus the flow

Received June 9, 1969; revision received October 3, 1969. This research was conducted at Auburn University in conjunction with the Master of Science in Aerospace Engineering program of J. L. Batson.
* General Engineer (Missiles), Research and Engineering Directorate; presently a graduate student in aerospace engineering at the University of Texas. Member AIAA.
† Professor of Aerospace Engineering. Member AIAA.

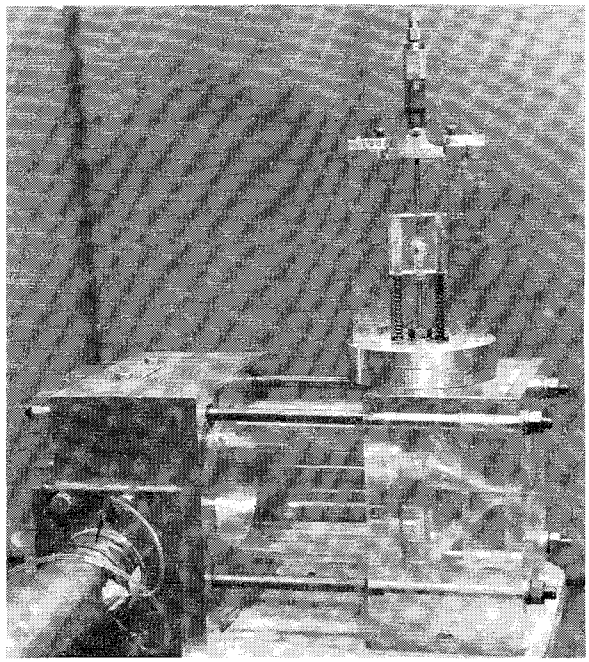

Fig. 1 Swirling flow chamber and nozzle with probe positioning device in place.

tangential velocity is introduced directly into the chamber. A dissimilarity arises, because inducing swirl by injecting gas tangentially to the chamber wall of a stationary model produces a tangential velocity gradient near the wall which may not exist near the surface of the cylindrical core grain, since the tangential velocity of the gas adjacent to the burning surface is approximately equal to the tangential velocity of the grain. However, as the flow approaches the throat in the SRM, the tangential velocity of the wall of the convergent section of the nozzle decreases as the throat is approached, whereas the velocity of the flow near the wall increases, due to Coriolis effects and area choking, causing a shearing action and a boundary layer.

Experimental Apparatus

The swirling flow chamber and nozzle are pictured in Fig. 1. The head plate and nozzle block were constructed from Plexiglas sheets. The chamber was a 6-in. length of Plexiglas tubing with a 4-in. internal diam and a 0.25-in. wall. The injection block consisted of a 2.5-in.-thick block of aluminum. A 0.5-in.-wide slot was machined tangentially to the chamber wall. At the outer edge of the block the slot was widened to accept the injection ports. Three injection ports corresponding to three swirl velocities were molded out of Fiberglas and resin. The purpose of these ports is twofold. They transfer the flow from a 2-in.-diam circular cross section to a rectangular cross section, and they provide a means of varying the tangential velocity by changing the inlet port area. Figure 2 shows the high-swirl injection port in place. The swirl apparatus was attached to the settling chamber of a supersonic wind tunnel (blow down type) air supply by a 2-in.-i.d. duct. The test installation provided a supply of dry air at essentially ambient temperature and at a regulated pressure.

Internal Flow Measurements and Visualization

All the internal flow experiments were conducted at an inlet total pressure of 80 psia and a nominal total temperature of 550°R. A pressure probe and an iron-constantan thermocouple were located in the settling chamber of the air supply. A Pitot pressure probe was situated in the 2-in.-i.d. inlet duct.

The swirl chamber internal flow measurements were obtained by small probes in a positioning device[1] (Fig. 1) which consisted of a Plexiglas slide which slid vertically in slots and held the probe. The depth of the probe was controlled by a Starret depth gage. The device also could be rotated on the azimuth ring which was affixed to the swirl motor. The internal flow of the medium swirl configuration was probed at three stations: in the plane of gas injection (station 1), in the cylindrical portion upstream of the nozzle convergent section (station 2), and in the convergent section of the nozzle (station 3).

At each station, the miniature probes[1,6] for flow direction, static pressure, stagnation pressure and stagnation temperature were introduced, one at a time, into the flow and traversed along the radius from the wall to the chamber axis. The probe used to determine flow direction was a 0.125-in.-diam stainless steel tube with two pressure orifices situated in a horizontal plane approximately 90° apart. Flow direction was obtained by slowly rotating the probe within the flowfield until the pressures on each orifice were equal. The flow direction would then bisect the angle between the orifices. A check was conducted with a flag probe.

The Pitot pressure probe was constructed from a polished 0.064-in.-diam stainless steel tubing with the end closed and a small hole drilled in the cylindrical portion of the tube. The stagnation temperature probe consisted of a 30-gage iron-constantan thermocouple inserted through 0.125-in. stainless steel tubing. The thermocouple was exposed to the flow by means of a rectangular aperature cut into the tubing. The static pressure was obtained by projecting an open-end, polished, stainless steel, 0.064-in.-diam tube into the flow. The static and stagnation pressure probes were calibrated at a Mach number of 0.14. Calibrations at higher Mach numbers were obtained by correcting for the effects of compressibility using the Karman-Tsien correction. The results are plotted in Fig. 3. With knowledge of the flow angle, Mach number and temperature, the tangential and axial velocities were calculated (Fig. 4). The radial velocity was not measured and was assumed to be small.

The flow was visualized in the swirl chamber by introducing a colored soap bubble solution and a kerosene paint pigment mixture at the injection block and photographing the resulting flow with an 8 mm movie camera at 48 fps and with a still camera. These investigations were conducted at a controlled total pressure of approximately 55 psia.

The tracer fluids were injected through the static pressure probe. It was found that the soap bubble solution would exit into the swirling flow when the probe was inserted to the axis of the swirl motor. This indicated a low pressure region at the axis of the swirl. Most of the solution was slung to the chamber wall where it would proceed along the wall in a helical path of near constant pitch until the convergent portion of the nozzle was reached. The pitch of the helix then increased until the fluid passed through the nozzle throat. Upon entering the divergent section, the pitch of the helical path abruptly decreased. A very small amount of the fluid was seen as a fog along the axis of the motor. The helical path of a paint pigment and kerosene mixture through the swirl motor is evident in Fig. 5. The swirl pattern in the

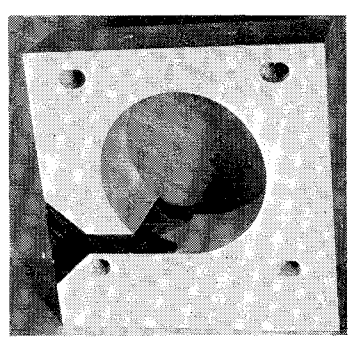

Fig. 2 High swirl injection port in place.

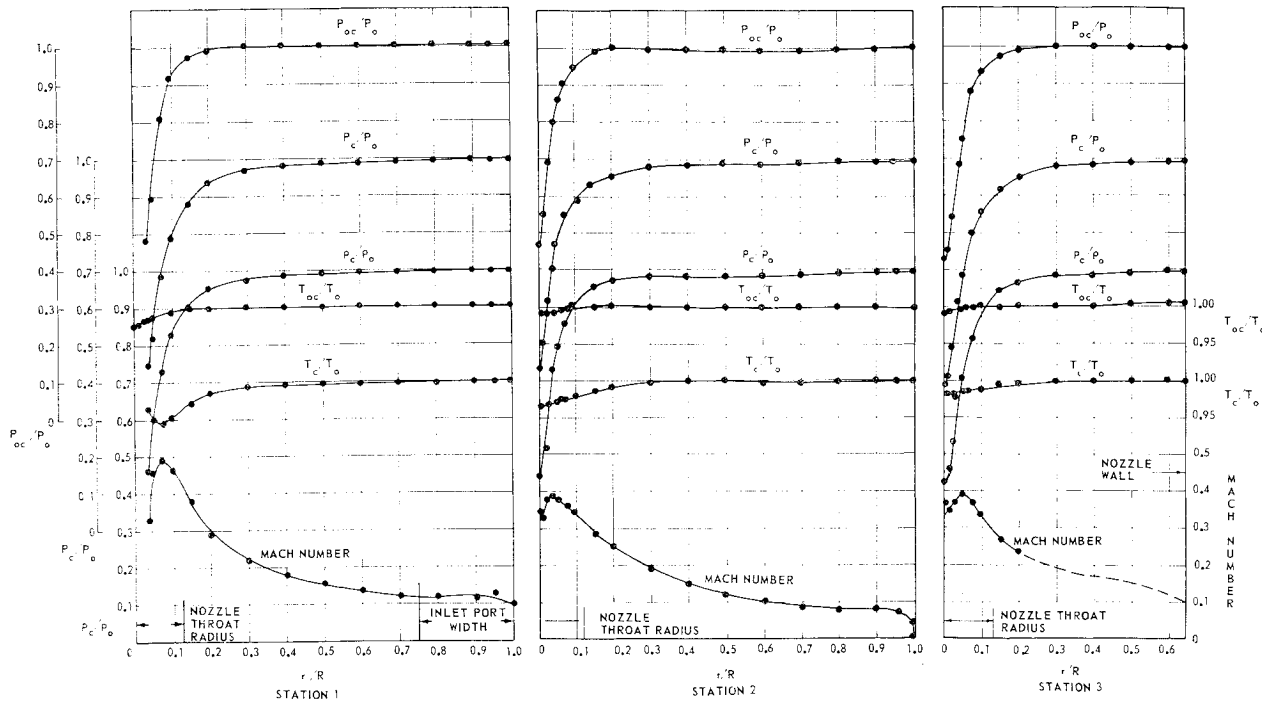

Fig. 3 Internal flow state properties at each station. (Read all pressure and density ratios to left; Mach number temperature ratios to right.)

nozzle convergent section is shown in Fig. 6. The flow on the head plate was of interest in that the flow direction was observed to be radially inward.

A tuft of wool was introduced into the flow and observed. Near the wall the tuft indicated a flow direction with a large circumferential component and a small axial component. This flow was probably caused by the boundary layer as indicated by the helix angle in the paint pigment tests. As the tuft was moved away from the boundary layer region, the axial component became negligible and the tuft behaved erratically, implying turbulent flow.

Internal Flow Characterization

Within the cylindrical portion three flow regimes exist (Fig. 7). In the wall boundary layer a small axial flow component coupled with a relatively large circumferential component is indicated by the helix angle in Fig. 5. In the convergent section of the nozzle, Fig. 6, the circumferential component increased as the throat was approached. After passing through the throat the axial component became large, with a corresponding decrease in the circumferential component. In the annulus region, between the wall boundary layer and the center portion, essentially two-dimensional flow existed with a large circumferential component, a negligible axial component and a small radially inward component. As the axis was approached, the flow acquired large circumferential and axial components with a small radially inward component. The radial velocity is zero on the axis.

The tangential velocity profile in the annulus region followed very closely the profile of a potential or inviscid vortex; i.e., the velocity varied approximately as $1/r$. The

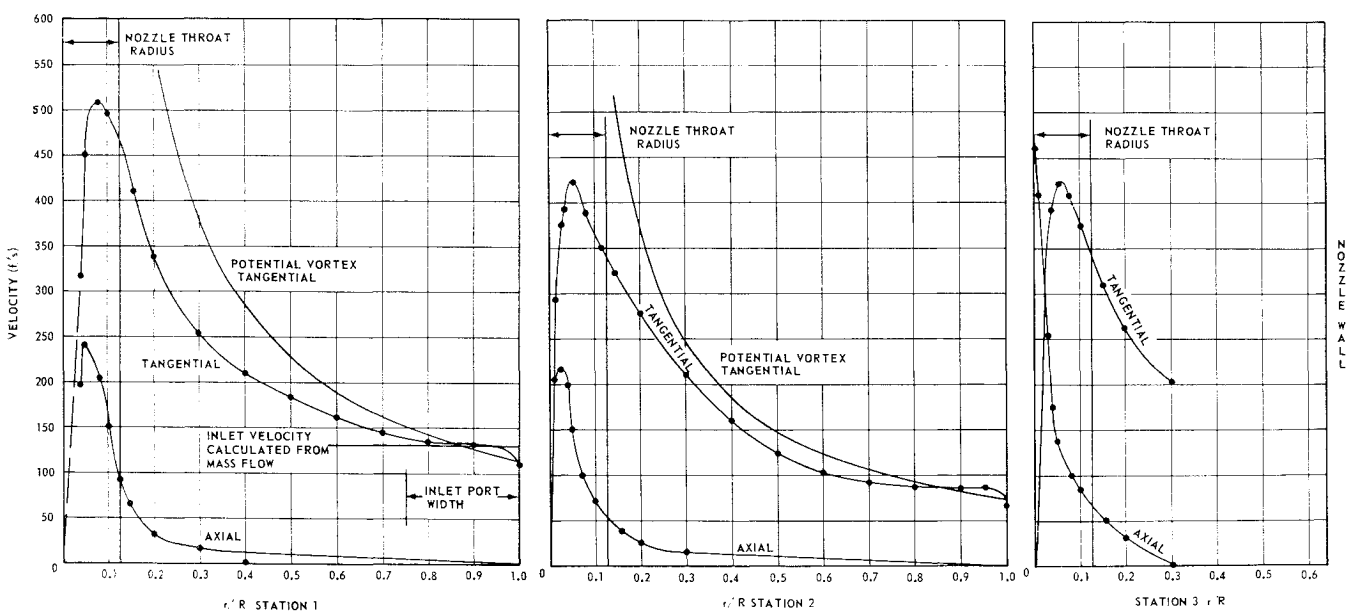

Fig. 4 Internal flow velocities at each station.

Fig. 5 Side view of swirl model showing flow pattern.

tangential velocity for potential vortex was traced on Fig. 4. Proceeding inward, the rate of increase of tangential velocity became less and less until the maximum velocity had been reached at $\partial v/\partial r = 0$. Proceeding further toward the axis, the tangential velocity decreased monotonically until at the axis the tangential velocity became zero. Thus the tangential flow in this region acted as solid body rotation.

The axial velocity indication in the annulus region was negligible. Proceeding inward the axial velocity became detectable at a position of about half the radius and increased at an increasing rate until the axis was reached.

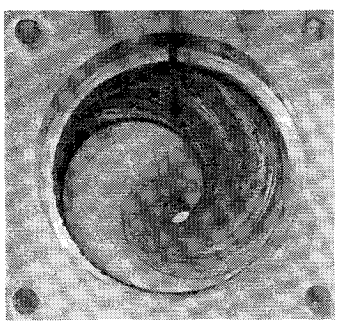

Fig. 6 Swirl pattern in nozzle convergent section.

The state properties—pressures, densities, and temperatures—in the flow were plotted in Fig. 3. The stagnation pressures remained essentially constant from the wall until a radius of approximately $r/R = 0.3$ was reached. From this point the stagnation pressure decreased rapidly as the axis was approached. The stagnation pressure drop occurred in the region of three-dimensional flow. In the cylindrical portion of the swirl motor the stagnation temperatures remained constant from the wall until the core region was reached. The stagnation temperature then markedly decreased in going toward the axis.

The stagnation temperature near the wall in the nozzle convergent section at station 3 was slightly higher than the total temperature of the incoming gas. Proceeding toward the axis, the total temperature became constant and equal to the incoming flow total temperature. Approaching the core, the total temperature decreased to its lowest value at the axis. The increase in total temperature occurred within the convergent section of the nozzle where the flow should be strongly three-dimensional is consistent with the Ranque-Hilsch effect.

Table 1 Exhaust flow measurement

Shadowgraph No.	Swirl	Injection total pressure, psia	r_c/r_e
1	Low	109	0.256
2	Low	81	0.413
3	Low	59	0.484
4	Medium	110	0.342
5	Medium	79	0.531
6	Medium	62	0.617
7	High	105	0.420
8	High	83	0.573
9	High	59	0.691

Exhaust Flow

The nozzle exhaust was examined by means of a shadowgraph. These investigations consisted of photographing the flow for various swirl conditions and control total pressures. The test conditions are listed in Table 1. Shadowgraph numbers 1, and 2 are depicted in Fig. 8. Note the center portion of the plume in each shadowgraph. The measured radius of the center portion or core is presented in Table 1.

The nozzle was designed to provide optimum expansion at a chamber pressure of 115 psia with axial flow. Since the experiments were conducted at chamber pressures less than 115 psia, the exhaust gases should be overexpanded. In order for the flow to adapt to atmospheric conditions, a shock should develop. A schematic of shadowgraph 1 of Fig. 8 is depicted in Fig. 9. This schematic presents an interpretation of the flow characteristics and shows the streamlines. A shock emanates as anticipated and is reflected from the free core stream as a centered expansion wave, and then is reflected from the free boundary. The flow in the stream core appeared to be subsonic in that shock waves in this region were not apparent.

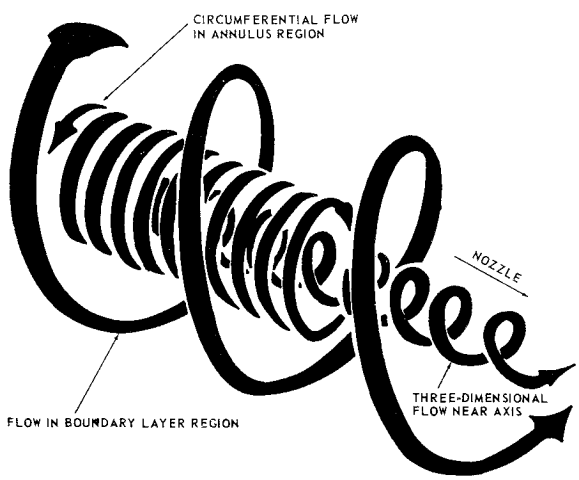

Fig. 7 Schematic of flow in swirl chamber.

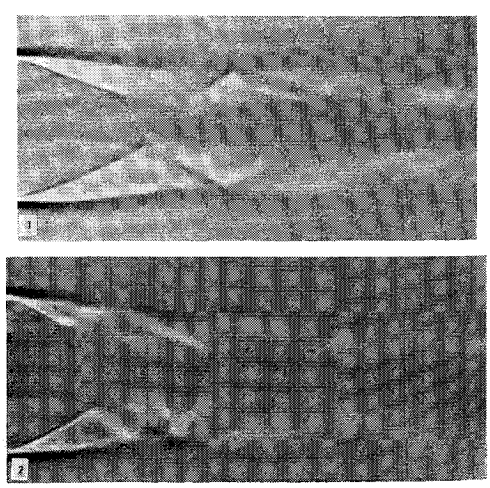

Fig. 8 Shadowgraphs of exhaust flow.

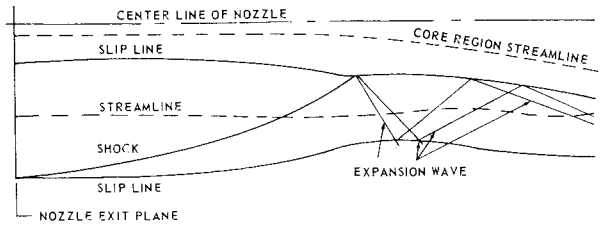

Fig. 9 Schematic of shadowgraph 1.

Shadowgraphs were made of the cylindrical portion of the chamber. The shadowgraphs showed a density discontinuity along the axis of the swirl motor. This core of radical density variation was very slender and approximately cylindrical. The core for the high swirl appeared to be larger in diameter than the core for medium swirl. The photos were of inferior quality and were not shown.

Mass Flow, Thrust, and Spin

Experiments were conducted with the injection stagnation pressure regulated at 80 psia and a stagnation temperature of 550°R. Mass flow was calculated from static and total pressure and temperature measurements in the inlet duct where the flow was essentially incompressible due to the low velocity. A reference spin rate was calculated from the tangential velocities near the wall at station 2, immediately upstream of the nozzle convergent section. By the tangential velocity near the wall the stagnation temperature and the nozzle throat radius, Mager's[8] swirl parameter, $\alpha^* = RV[(\gamma - 1)/2]^{1/2}/r^*a_o$, was determined for each of the three swirl conditions. Mass flow measurements are plotted vs α^* in Fig. 10. Both mass flow and thrust decrease drastically with an increase in α^*. The experimental data closely approximate Mager's solution at the conditions considered; however, the mass flow deviation increases as α^* is increased. The thrust measurements were obtained by the use of strain gages mounted on the inlet duct. Measurements were obtained for the three swirl conditions and axial flow.

Binnie, Hookings, and Kamel[9] conducted experiments with the flow of swirling water (incompressible case) through a nozzle and found good agreement with potential flow theory at low swirl. Their results also showed a deviation from theory with increased swirl.

Conclusions

The Ranque-Hilsch method of producing swirling flows is useful for research of swirling flow through a nozzle. A simple and inexpensive apparatus has been constructed for creating swirl. The device makes measurements and visualization of internal flow characteristic, as well as determination of thrust and mass flow, practical. The results may be applied to analyses of effects produced in cylindrical core spinning rocket motors only with caution as boundary layer effects in solid propellant rockets are different and similarity relationships between hot and cold flows have not been established.

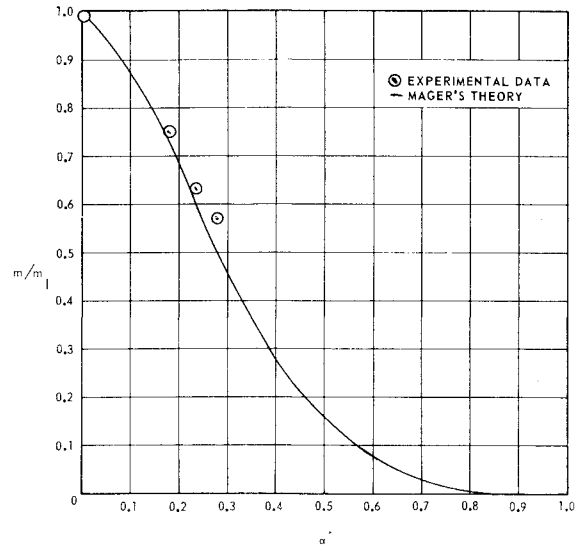

Fig. 10 Comparison of experimental mass flow with Mager's predicted curve.

For the swirl conditions considered, Mager's isentropic theory for swirling flows was essentially substantiated. Supersonic swirling flow produced by the nozzle represents an area of basic interest for further research.

References

[1] Lay, J. E., "An Experimental and Analytical Study of Vortex-Flow Temperature Separation by Superposition of Spiral and Axial Flows," *Journal of Heat Transfer*, Vol. 81, No. 3, Aug. 1959, pp. 202–222.

[2] Hartnett, J. P. and Eckert, E. R. C., "Experimental Study of the Velocity and Temperature Distribution in a High Velocity Vortex Type Flow," *Preprints of Proceedings of 1956 Heat Transfer and Fluid Mechanics Institute*, Stanford Univ. Press, Stanford, Calif., June 1956, pp. 135–150.

[3] Deissler, R. G. and Perlmutter, M., "Analysis of the Flow and Energy Separation in a Turbulent Vortex," *International Journal of Heat and Mass Transfer*, Vol. 1, No. 213, Aug. 1960, pp. 173–191.

[4] Kassner, R. and Knoernschild, E., *Friction Laws and Energy Transfer in Circular Flow*, TR. F-TR-2198-ND, 1947, Wright-Patterson Air Force Base, Ohio.

[5] Van Deemter, J. J., "On the Theory of the Ranque-Hilsch Cooling Effect," *Applied Scientific Research*, Vol. A3, No. 3, 1951, pp. 174–196.

[6] Dean, R. C., *Aerodynamic Measurements*, 1st ed., Gas Turbine Lab., Massachusetts Institute of Technology, Eagle Enterprises, Boston, 1953, pp. 27–156.

[7] Shapiro, A. H., *The Dynamics and Thermodynamics of Compressible Fluid Flow*, 1st ed., Vol. I, Ronald Press, New York, 1953, pp. 341–349.

[8] Mager, A., "Approximate Solution of Isentropic Swirling Flow Through a Nozzle," *ARS Journal*, Vol. 31, No. 8, Aug. 1961, pp. 1140–1148.

[9] Binnie, A. M., Hookings, G. A., and Kamel, M. Y. M., "The Flow of Swirling Water Through a Convergent-Divergent Nozzle," *Journal of Fluid Mechanics*, Vol. 3, No. 3, Dec. 1957, pp. 261–274.